A Comparison of Multicopter Noise Characteristics with Increasing Number of Rotors

Brendan Smith
PhD Student

Dr. Farhan Gandhi
Redfern Chair, Director

Dr. Robert Niemiec
Research Scientist

Center for Mobility with Vertical Lift (MOVE)
Rensselaer Polytechnic Institute
Troy, New York, United States

ABSTRACT

This study examines the acoustic behavior in hover of manned-size, multi-rotor, eVTOL aircraft in the classical quadcopter, hexacopter and octocopter configurations. The rotors are assumed to have collective pitch control and operate at a specified RPM, with orthogonal and tip-to-tip rotor phasing considered. All configurations have the same disk loading and tip Mach number, with the rotor radius decreasing and RPM increasing, going from the quadcopter to the octocopter. The simulations use the Rensselaer Multicopter Analysis Code (RMAC) for the aerodynamic loads on the blades, coupled to PSU-WOPWOP for predictions of propagated noise. From the simulation results, orthogonal phasing between rotors is shown to produce significant noise reductions along inter-boom bisectors (between 9-14 dB relative to an equivalent single rotor, at 6lb/ft^2 disk loading and 0.51 tip Mach number). Further reducing the tip Mach number not only reduces the propagated noise but produces even deeper regions of quiet along the inter-boom bisectors (18-25 dB quieter at 3lb/ft^2 with 0.36 tip Mach number). An examination of the overall sound pressure frequency spectra indicates that smaller faster spinning rotors (going from the quadcopter to octocopter) produce more tonal peaks at higher frequencies which results in penalties in A-weighted noise.

1. INTRODUCTION

With the emergence of distributed electric propulsion as a key enabling technology viable at a larger scale, there has been tremendous interest in recent years in the development of multi-rotor electric Vertical Takeoff and Landing (eVTOL) aircraft. While battery powered, electric motor driven, small multi-copters have been available to hobbyists, videographers, and recreational users for quite some time, there is now a strong push toward the development of *manned-size* eVTOL aircraft in support of the Urban Air Mobility (UAM) vision, as promoted through the likes of the Uber Elevate Program (Ref. 1), the NASA UAM Grand Challenge (Ref. 2, 3), and the establishment of many strategic partnerships and a UAM ecosystem. The success of the UAM vision, relying on the ubiquitous use of manned-size eVTOL aircraft to quickly and efficiently ferry people and goods across the urban/suburban landscape, however, requires overcoming several major technical and logistical challenges.

Key among the technical challenges is the noise generated by eVTOL aircraft operating in areas of high population density, and its impact on community acceptance. Sustained work over the last several decades has resulted in an excellent understanding of the aeroacoustic charactersitics of conventional helicopters. For example, Ref. 4 explains the key noise sources – thickness noise, loading noise, high-speed impulsive noise, and blade-vortex interaction noise – on conventional helicopters, and the conditions in which they dominate. However, a similar degree of understanding is currently lacking for multi-rotor eVTOL aircraft.

To address this gap, the Aeroacoustics Branch at NASA Langley Research Center (LaRC) has undertaken a significant campaign focusing on experimental studies as well as associated simulations and analysis on small, fixed-pitch, variable-RPM rotors and their assemblies (Refs. 5-9). Their studies examine, in detail, the noise contributing sources, rotor-airframe interaction effects, broadband noise, and the effect of phase synchronization between rotors. Additional studies of acoustic measurements on small, fixed-pitch, variable-RPM single rotors, quadcopters and hexacopters, recently conducted by other academic groups, are reported in Refs. 10-12.

Several simulation studies on acoustics of multi-rotor aircraft have also been conducted in recent years. Unlike the experimental studies in the previous paragraph on small rotors, many of these simulations focus on larger multi-rotor aircraft with a greater direct relevance to Urban Air Mobility applications and missions. Passe and Baeder (Ref. 13) studied the effect of rotor design parameters and boom shadow on eVTOL aeroacoustic characteristics in hover

Presented at the Vertical Flight Society's 76th Annual Forum & Technology Display, Virginia Beach, Virginia, October 6-8, 2020.

conditions. Quackenbush et al., (Ref. 14) and Jia and Lee (Ref. 15), analyzed the acoustics characteristics of very specific configurations currently under study in the eVTOL community, such as Piasecki's slowed rotor wing-compounded eVTOL design, and NASA's 1- and 6-passenger concept quadrotor eVTOL designs. Another area that is receiving much attention lately is the aeroacoustic implications of propeller-wing, -body, -duct, and -boom interactions (Refs. 13, 16-18) likely to be encountered on typical eVTOL aircraft. Similarly, there is high interest in broadband noise of variable-RPM eVTOL rotors (Refs. 7, 19, 20), since this has identified to be a more important noise source than seen on traditional helicopter rotors (Refs. 5, 10).

There are also other factors to consider in eVTOL aircraft development that can ultimately have implications on aeroacoustics. While small multi-copters are all controlled using variable-RPM rotors, recent studies suggest that as the rotor diameter increases, variable-RPM control alone may be unable to meet handling qualities requirements, specifically falling short in disturbance rejection capabilities (Refs. 21-24). Collective pitch control on individual rotors offers one solution to this challenge, and as an example, Joby Aviation's 4-passenger S4 aircraft (Ref. 25), includes this feature. The presence of collective pitch control, in turn, allows for potential phase synchronization between various rotors operating at the same speed. References 26 and 27 have already explored the use of rotor phasing for eVTOL aircraft vibration reduction, and there is also the potential to further develop on the ideas in Refs. 8 and 9 for improved aeroacoustics of large eVTOL aircraft.

With this background, the current study examines the aeroacoustic characteristics of UAM-scale, multi-rotor eVTOL aircraft in hover, specifically comparing the influence of number of rotors and variation in disk loading (through change in tip Mach number or rotor root pitch) on noise levels and radiated acoustic energy. With each rotor operating at the same RPM, the effect of rotor-to-rotor phasing is considered, and the study places a strong emphasis on understanding the interference behavior from multiple coherent acoustic sources, which the individual rotors present.

2. ANALYSIS

The rotor aerodynamic loads for the multi-rotor configurations considered in the present study are evaluated using the Rensselaer Multicopter Analysis Code (RMAC), a physics-based comprehensive and flight-simulation analysis tool described in Ref. 28. RMAC uses blade-element-theory, in conjunction with a 10-state Peters-He finite-state dynamic wake model to calculate the blade sectional aerodynamic loads which can be integrated along the span and around the azimuth to obtain the rotor loads. While RMAC has the capability to model the rotor blades as rigid, or undergoing elastic deformation, the rigid blade option is exercised in the current simulations.

Three different multi-copter configurations – a classical quadcopter, a classical hexacopter, and a classical octocopter – each with two-bladed rotors, are considered in hover conditions. Two different rotor phasing scenarios for each multi-copter are examined, as shown in Figures 3, 12, and 17. With *orthogonal phasing*, the blade-tip to blade-tip distance between adjacent rotors is a maximum, while *tip-to-tip phasing* results in that distance being a minimum. As the figures indicate, tip-to-tip phasing has the blades of each rotor positioned normal to their corresponding boom axis at the same instant during every revolution. With orthogonal phasing, when alternate rotors (say the counter-clockwise rotors) have their blades positioned normal to their booms, the adjacent rotors (the clockwise rotors) have their blades aligned along their booms at the same instant during every revolution.

To enable fair comparisons across the multi-copter configurations, the non-dimensional rotor geometric parameters and airfoils are identical (rotor solidity of 0.0646, blade linear twist of –12 deg/span, linear taper with a tip chord/root chord of 0.75, and a linear blend of airfoils from a NACA 2412 at the blade root to a Clark Y at the tip). The nominal aircraft gross weight is 1206 lbs, and the nominal blade root pitch (to achieve the required thrust to hover) is 18.8 deg, across multi-copter configurations. The total disk area across configurations is the same (maintaining a nominal disk loading of 6 lb/ft^2), so the rotor radius progressively decreases going from the quadcopter to the octocopter. The boom length for each configuration is set such that the tip clearance between the rotors is 10% of the rotor's radius. The tip Mach number (nominally at 0.51) is unchanged across configurations, so the rotor RPM increases going from the quadcopter to the octocopter. Variation in rotor radius and RPM across multi-copter configurations are presented in Table 1. Also considered for comparison is an *equivalent single rotor* with twice the radius of the quadcopter rotors and operating at half the RPM of the quadcopter rotors. Thus the equivalent single rotor has the same disk loading and tip Mach number as the multi-copter configurations. Its radius is denoted as R_o.

The blade loads from each rotor are provided as inputs to PSU-WOPWOP (Ref. 29), an acoustic propagation code based on the numerical implementation of Farassat's Formulation 1A of the Ffowcs Williams and Hawkings (FW-H) equation. RMAC provides chordwise compact loads to PSU-WOPWOP, and only the discrete frequency (tonal) noise from thickness and loading sources are considered in the acoustic analysis. PSU-WOPWOP calculates the acoustic pressure time history at observer locations selected by the user, coming from the specified number of rotors (whose positions, and relative rotor phasing is also specified). In the present study, observers are placed on a 100 ft radius hemisphere (12.5 times the equivalent single rotor radius, R_o, and distant enough to be in the acoustic far-field) in 5 deg increments in both azimuth and elevation angle, as shown in Figure 1. The overall sound pressure level (OASPL) in dB

and dBA are calculated from the acoustic time pressure histories.

Also calculated, for comparison across various configurations, is the total acoustic power radiated (PWL) over the observer hemisphere. First the sound intensity normal to the individual observers is calculated from the acoustic pressure history using

$$I = \frac{p^2}{\rho c} \quad (1)$$

where p^2 is the mean square pressure at the observer, ρ is air density, and c is speed of sound.

The radiated acoustic power (PWL), for any configuration, is obtained by integrating the sound intensity calculated above over the surface of the hemisphere. However, the radiated acoustic power results presented in the current study are normalized with respect to the equivalent single rotor as follows:

$$PWL_{dB} = 10 * \log_{10}\left(\frac{PWL_{multicopter}}{PWL_{equivalent\ single\ rotor}}\right). \quad (2)$$

3. VALIDATION

The present simulation method (with RMAC blade load predictions coupled to the PSU-WOPWOP acoustic propagation code described in Section 3) is first validated against experimental and simulation results from NASA Langley Research Center reported by Schiller et. al (Ref. 8). In Ref. 8, a two-rotor system was considered, with rotors operating in both co-rotating and counter-rotating configurations, and with a relative phasing of 0° and 90°. Each rotor was two-bladed, had a diameter of 0.317m, and a clearance of 0.083m between the rotor disks. Microphones were placed over a 1.9m radius partial hemisphere at five equally spaced observer stations between elevation angles of 0° (in-plane) and –45°, and moved in 11.25° increments (corresponding to 32 points) around the azimuth. Rotor operational details for the present simulation (RPM, thrust, etc.) were matched to those reported in Ref. 8. As was done with the NASA Langley experimental data, only the spectral energy within a ±10 Hz window around the blade passage frequency was considered when evaluating the sound pressure level.

Figure 2 shows a comparison of the sound pressure level predictions in the plane of the rotors for four different cases (representing differences in direction of rotation and rotor phasing). The cloverleaf shape observed in the counter-rotating pairings in the NASA experiments and simulations are captured accurately by the present simulations. The corotating pairs also match well, with the almost axisymmetric shape observed for 0° relative phasing and dipole like shape for 90° phasing well captured. Next, predictions of acoustic power radiated through the partial hemisphere (described in the previous paragraph) are compared to results from Ref. 8. Like Ref. 8, the radiated power reported is normalized by double the intensity from an isolated single rotor, and the results are presented in Table 2. The present simulations show good correlation with experiment and excellent correlation with the NASA Langley simulations for co-rotating rotor pairs (which display large increase or decrease in radiated acoustic power, depending on relative rotor phasing). Although the radiated power for counter rotating rotors shows some difference, it should be noted that the values are very small (compared to results for the co-rotating rotors), indicating that the radiated acoustic power from the counter-rotating pairs over the partial hemisphere is essentially very similar to twice that radiated by the single rotor operating in isolation. In summary, the validation results in Figure 2 and in Table 2 provide good confidence in the simulation tools used in the present study.

4. RESULTS

4.1 Quadcopter

Figure 3 shows a quadcopter with orthogonal and tip-to-tip rotor phasing, and Figure 4 shows the overall sound pressure level (OASPL) on hemispheres of radius 12.5R_o for these two cases. With orthogonal phasing, large reductions in noise are observed along the inter-boom directions. The noise reductions are greatest along the rim of the hemisphere (or at 0° elevation, in the plane of the rotors), and decrease with increasing elevation angle. Figure 5 compares the OASPL in the rotor plane (0° elevation) for the orthogonal and tip-to-tip phasing cases, with the OASPL of the single rotor also shown, as a reference. In Figure 5, while the in-plane noise generated by the quadcopter with tip-to-tip phasing is consistently between 1-3 dB lower than that of the corresponding single rotor (regardless of azimuthal position), the noise along one inter-boom bisector for the quadcopter with orthogonal phasing is up to 9dB lower than the single rotor. Reductions of 5dB are observed along the other inter-boom bisector. The following paragraphs investigate the reasons for these differences.

Figure 6 shows the acoustic pressure signal at an in-plane observer location on the hemisphere from a single rotor of the quadcopter situated at the origin of the hemisphere. Note that counter-clockwise and clockwise spinning rotors produce identical acoustic pressure signals, characterized by two negative impulsive peaks over a given rotor revolution. If a counter-clockwise and a clockwise rotor, with *tip-to-tip rotor phasing*, were hypothetically superposed at the origin, the acoustic pressure peaks from each rotor would arrive at the observer at the same instant, resulting in the amplification of the individual rotor signals (Figure 7). On the other hand, if the superposed counter-clockwise and clockwise rotors are *orthogonally phased*, the acoustic pressure signals from each individual rotor have a quarter revolution phase difference and produce a combined signal with a 4/rev fundamental frequency (instead of 2/rev for the tip-to-tip phasing), as seen in Figure 8.

Next we examine the case of laterally offsetting the *orthogonally-phased* coincident counter-clockwise and clockwise rotors previously considered in Figure 8. There are two possible configurations as shown in Figure 9. The *bearhug*, where the counter-clockwise rotor is offset right and the clockwise rotor offset left by an identical distance; and the *breaststroke*, where the positions are reversed. While the contributions of the individual rotors to the acoustic pressure time history at the observer are identical (other than a quarter revolution phase shift), it is to be noted that the breaststroke, with the advancing blades of both rotors closer to the observer, results in an earlier arrival of the acoustic pressure peaks. In contrast, the bearhug, with the advancing blades farther from the observer, results in a later arrival of the acoustic pressure peaks. The temporal offsets of the acoustic pressure peaks are to either side of those seen in Figure 8 (where the counter-clockwise and clockwise rotors were coincident at the origin).

In Figure 4, counter-clockwise rotors are shown in blue and clockwise rotors are shown in red. For observers A and C, the bearhugging rotor-pair appears closer and the breaststroking rotor pair is situated further back. In contrast, the order is reversed for observers B and D. Figure 10 shows the acoustic pressure signal at observer A from the front bearhugging rotor pair, the rear breaststroking rotor pair, as well as the sum. The acoustic pressure peaks from the rear pair arrive later than those from the front pair (due to greater travel distance), but the temporal offset is reduced in part by the phenomena explained in Figure 9 (that peaks from a bearhugging rotor pair arrive a little later than those from a breastroking rotor pair travelling the same distance). Similarly, Figure 11 shows the acoustic pressure signal at observer B from the front breaststroking pair, the rear bearhugging pair, and the sum. In contrast to Figure 10, the temporal offset between the front and rear rotor acoustic pressure peaks is increased since the front breast-stroking peaks arrive at the observer extra early, and the rear bearhugging peaks have an extra delay. The relative phasing results in a lower amplitude total acoustic pressure signal at observer A (or C), seen in the black curve in Figure 10, compared to an observer at B (or D) (as seen black curve on Figure 11). These lower amplitude acoustic waves at observers A and C (compared to B and D), in turn result in quieter regions observed on Figures 4 and 5 for orthogonally phased rotors.

It should be noted that although the quadcopter with orthogonally phased rotors produce pronounced low noise regions along the inter-boom bisectors (relative to rotors with tip-to-tip phasing), the integrated noise over the hemisphere is comparable to that generated over for the quadcopter with tip-to-tip phasing. Normalizing the data by that of the equivalent single rotor, the orthogonal quadcopter has PWL of -0.74 dB, and the tip-to-tip a value of -0.64 dB, showing that the net radiated power levels are close to one another for the two rotor phasing configurations.

4.2 Hexacopter and Octocopter

As with the quadcopter in the previous section, the present section examines the acoustic characteristics of a hexacopter and an octocopter. Figure 12 shows a hexacopter with orthogonal and tip-to-tip rotor phasing, and Figure 13 shows the corresponding overall sound pressure level (OASPL) on $12.5R_o$ radii hemispheres. In Figure 13, tip-to-tip rotor phasing shows considerably higher peak noise levels than orthogonal phasing. In Figure 4, in comparison, the quadcopter's peak noise levels did not differ appreciably between the tip-to-tip and orthogonal phasing cases, although the latter displayed regions of relative quiet along the inter-boom directions. Figure 14 shows the in-plane OASPL for the hexacopter (at 0^o elevation, along the rim of the hemispheres). From this figure, noise reductions of up to 9.5 dB (relative to the equivalent single rotor) are observed along alternate inter-boom bisectors (at 60^o, 180^o, and 300^o) in the case of orthogonal rotor phasing. From Figure 12 it can be seen that at these quiet observer locations, the nearest rotors are a bear-hugging rotor pair. Along the other inter-boom bisectors (at 0^o, 120^o, and 240^o), when the nearest rotors to the observer are a breast-stroking rotor pair, Figure 14 shows that the noise levels are comparable to (within 1 dB of) equivalent single main rotor levels. In this regard, the hexacopter differs from the quadcopter, which showed substantial in-plane noise reductions along all inter-boom bisectors. From a comparison of Figures 14 and 5, the in-plane noise of the hexacopter with tip-to-tip rotor phasing also differs substantially from that produced by the quadcopter with tip-to-tip phasing. While the tip-to-tip quadcopter showed no particular acoustic directionality in Figure 5, the tip-to-tip hexacopter shows in-plane noise lows comparable to those of the orthogonally phased hexacopter, and along generally similar directions (see Figure 14). Along the 0^o, 120^o, and 240^o inter-boom bisectors, on the other hand, with the breast-stroking rotor pair closest to the observer, the tip-to-tip phasing produces a 7 dB noise increase over the equivalent single main rotor.

Figure 15 shows the acoustic pressure signal over a single rotor revolution along the hexacopter's 180^o inter-boom bisector. With orthogonal rotor phasing, each rotor pair (the nearest bear-hugging pair 1-2, the intermediate breast-stroking pair 3-6, and the farthest bear-hugging pair 4-5) produces a 4/rev signal at the observer, and the relative phasing of the individual signals is such that the total acoustic pressure signal has a relatively low amplitude. With tip-to-tip rotor phasing, each individual rotor pair produces a 2/rev signal at the observer, but the relative phasing once again produces a relatively low amplitude total acoustic pressure signal. Figure 16 shows similar results along the 120^o inter-boom bisector. For orthogonal phasing, the 4/rev acoustic pressure signals from individual rotor pairs (the nearest breast-stroking pair 1-6, the intermediate bear-hugging pair 2-5, and the farthest breast-stroking pair 3-4) are relatively phased such as to generate a larger amplitude total acoustic pressure signal (compared to Figure 15 along the 180^o inter-boom bisector). Likewise, for tip-to-tip phasing, the 2/rev

acoustic pressure signals from individual rotor pairs are relatively phased such as to generate a much larger amplitude total acoustic pressure signal (which in turn generates 7 dB higher noise than the single rotor, as seen in Figure 14).

Next, Figure 17 shows an octocopter with orthogonal and tip-to-tip rotor phasing, and the corresponding overall sound pressure levels on $12.5R_o$ radii hemispheres are shown in Figure 18. In Figure 18, although the peak noise levels with tip-to-tip rotor phasing are comparable to those with orthogonal phasing, the tip-to-tip phasing generates significantly higher overall noise (characterized by larger areas of high noise on the hemisphere). The octocopter hemispheres show characteristics similar to those for the quadcopter in Figure 4, with significant noise reductions along all inter-boom bisectors. At 0^o elevation, along the rim of the hemispheres, Figure 19 shows 13-14 dB reductions in in-plane OASPL along the inter-boom directions for the orthogonal phasing case, relative to the single main rotor. For the same phasing, noise increases of up to 2.5 dB are observed along the boom directions. With tip-to-tip phasing, the octocopter generates between 2-4 dB higher in-plane noise, relative to the single main rotor.

Figures 20 and 21 show the acoustic pressure signals over a single rotor revolution along the octocopter's 180^o and 135^o inter-boom bisectors, respectively. With orthogonal rotor phasing, each rotor pair (starting with the nearest bear-hugging pair 1-2 for Figure 20, and the nearest breast-stroking pair 1-8 for Figure 21) produces a 4/rev signal at the observer, and for both observer locations, the relative phasing of the individual signals is such that the total acoustic pressure signal has a relatively low amplitude. As seen previously in the case of the hexacopter in Figures 15 and 16, with tip-to-tip rotor phasing each individual rotor pair produces a 2/rev signal at the observer, but the relative phasing does not result in a total acoustic pressure signal of reduced amplitude (as was the case with orthogonal phasing).

4.3 Multi-copter Comparison

Following the results presented in sections 4.1 and 4.2, the current section seeks to compare the different multi-copter configurations. Figure 22 shows the frequency spectra of the overall sound pressure level at an in-plane observer in front of the aircraft ($\Psi = 180^o$). The quadcopter, hexacopter, and octocopter results in Figure 22 are for orthogonal phasing, and in each case $\Psi = 180^o$ corresponds to an inter-boom direction of low radiated noise. As compared to the single rotor where all the tonal peaks appear to be confined to frequencies of under 300 Hz, multi-copters with increasing numbers of rotors (and correspondingly higher operating RPMs) show tonal peaks at progressively higher frequencies. Also shown on the figure is the A-weighting curve up to a frequency of 1000 Hz. Clearly, an A-weighted overall sound pressure level calculation would most penalize the octocopter (with the highest blade passage frequency of all the configurations and higher tonal peaks at higher frequencies).

Next, Table 3 presents the acoustic power radiated over the entire observer hemisphere (PWL), for the various multi-copter configurations. The results, presented for both orthogonal as well as tip-to-tip phasing, are normalized with respect to the equivalent single rotor. For the quadcopter, it is interesting to note that while results in Section 4.1 showed strong directivity with orthogonal phasing (absent for tip-to-tip phasing), the total radiated acoustic power over the hemisphere does not show much difference between the orthogonal and tip-to-tip phasing and is in both cases lower than the equivalent single rotor. However, this is not the case for the hexacopter and octocopter, where orthogonal phasing shows a reduction in PWL relative to the equivalent single rotor, but tip-to-tip phasing shows an increase. A –0.74 dB reduction in Table 3 for the orthogonal quadcopter represents a 15% lower PWL, while a +2.02 dB increase for the tip-to-tip octocopter represents a 59% higher PWL, relative to the equivalent single rotor.

Table 4 presents similar results to Table 3, but with the application of A-weighting to the calculation of radiated acoustic power. Both orthogonal and tip-to-tip phasing have higher radiated acoustic energy relative to the equivalent single rotor, when A-weighting is considered, and the radiated energy progressively increases going from the quadcopter to octocopter. An 8.16 dB result for the orthogonal quadcopter corresponds to a 550% increase in radiated acoustic energy relative to the equivalent single rotor, while a 15.07 dB result for the tip-to-tip octocopter represents a 3200% increase in acoustic energy.

4.4 Variation in Disk Loading

While the previous sections presented acoustics results for multi-copters at a $6lb/ft^2$ disk loading, the present section examines the effect of change in disk loading on the acoustic characteristics of the quadcopter. The quadcopter rotor geometry is unchanged from that described in section 2, and its radius held fixed at 4 ft as reported in Table 1. The disk loading is changed either through variation of tip speed, or through variation of root pitch. Figure 23 shows contours of constant disk loading, as a function of tip Mach number and geometric root pitch. Five specific points on Figure 23 are considered for comparison. Point A (with tip Mach number of 0.51 and root pitch of 18.8 deg) was already extensively examined in section 4.1. Points B and C correspond to rotors with the same root pitch operating at increased tip Mach numbers of 0.6 and 0.685, respectively, with corresponding disk loading values of $9lb/ft^2$ and $12lb/ft^2$. Points D and E correspond to a tip Mach number of 0.6, with root pitch values of 15.9 deg and 22.5 deg. Points D, B, and E, as a set, represent an increase in disk loading from $6lb/ft^2$ to $9lb/ft^2$ to $12lb/ft^2$, through increase in blade root pitch while holding the tip Mach number constant. An additional point, F, is considered along with the set A, B, C, where the tip Mach number is further reduced to 0.36 to realize a disk loading of $3lb/ft^2$ disk (while holding root pitch at the nominal value of 18.8 deg, as with points A, B, and C).

Figure 24 shows the in-plane OASPL for the points F, A, B, and C, respectively. Also shown on the figures is the noise generated by an equivalent single main rotor. Note that the single main rotor's tip speed on each of the plots is varied to be equal to that of the corresponding quadcopter. The noise directionality (with inter-boom lows) previously observed for the orthogonally phased quadcopter at 6lb/ft^2 is not evident at the higher disk loading values (9lb/ft^2 to 12lb/ft^2). At 9lb/ft^2 the quadcopter in-plane OASPL falls within 3dB of the single main rotor, for both rotor phasing cases considered. Similarly, at 12lb/ft^2 in-plane OASPL values lie between –3dB to +1.5dB of the single rotor levels. At the low 3lb/ft^2 disk loading, however, the noise directionality with orthogonal phasing is even stronger than observed at the moderate 6lb/ft^2 loading, with the OASPL along the inter-boom bisectors between 18-25dB lower than the single rotor. In addition to the orthogonally phased quadcopter's noise directionality (stronger at lower disk loadings) or lack thereof (at higher disk loading), the in-plane noise level, itself, rises significantly when disk loading is increased through increase in tip Mach number. Specifically, the single rotor in-plane OASPL increases from 72dB at 3lb/ft^2 (with tip Mach number 0.36), to 86dB at 6lb/ft^2 (with tip Mach number 0.51), to 92dB at 9lb/ft^2 (with tip Mach number 0.6), to 98dB as the disk loading increases from 12lb/ft^2 (at tip Mach number 0.685), with the quadcopter peak noise levels comparable to the single rotor at the same disk loading.

Next, Figure 25 shows the in-plane OASPL for the points D, B, and E, respectively, with the equivalent single rotor again included for reference. With the tip Mach number held at 0.6, when the disk loading is increased from 6lb/ft^2 to 9lb/ft^2 to 12lb/ft^2 by increasing root pitch from 15.9 deg to 18.8 deg to 22.5 deg the single rotor OASPL shows a much smaller 3dB change, from 90dB to 92dB to 93dB. Recall that in comparison, when disk loading was increased over the same range by holding the pitch at 18.8 deg and increasing tip Mach number from 0.51 to 0.685, the single rotor in-plane OASPL increased by 12dB (from 86dB to 98dB). In Figure 25, the quadrotor in-plane OASPL levels lie between –3dB to +1dB of the single rotor, for both orthogonal and tip-to-tip phasing, with no evidence of strong noise directionality observed at lower Mach numbers (0.36 and 0.51), even at 6lb/ft^2 disk loading.

For variation in tip Mach number and disk loading conditions corresponding to points F, A, B, and C, Figure 26 shows the acoustic pressure signals at an in-plane inter-boom (90 deg) location, for orthogonal rotor phasing. Also shown on the figure are noise decompositions into thickness and loading contributions. As the disk loading increases, the thickness noise progressively increases as a fraction of the total noise, and at higher tip Mach numbers (0.6 for point B, and 0.685 for point C), thickness noise becomes the dominant source. For variation in root pitch and disk loading conditions corresponding to points D, B, and E, Figure 27 shows the acoustic pressure signals, and decomposition into contributing sources, at the same observer location, and for the same orthogonal rotor phasing. At tip Mach number 0.6, at lowest pitch (and disk loading), the thickness noise dominates. With the tip Mach number unchanged and root pitch increased to increase disk loading, the loading noise is observed to progressively increase, and increases to levels comparable to the thickness noise at 12lb/ft^2 disk loading.

5. CONCLUSIONS

This study examines the acoustic behavior of manned-size, multi-rotor, eVTOL aircraft with four, six, and eight rotors (arranged in classical quadcopter, hexacopter and octocopter configurations), in hover. The rotors were assumed to have collective pitch control and operate at a specified RPM, with the ability to control phasing between the rotors. Two specific phasing scenarios, referred to as orthogonal and tip-to-tip, were considered in the study. The nominal aircraft weight was 1206 lbs, and the total rotor disk area and rotor tip speed for all configurations was the same, corresponding to a nominal disk loading of 6lbs/ft^2, and tip Mach number of 0.51. The larger rotors of the quadcopter had a 4 ft radius and nominally operated at 1371 RPM, while the smallest rotors of the octocopter had a 2.83 ft radius and operated at 1939 RPM. The aerodynamic loads on the rotor blades were calculated using the Rensselaer Multicopter Analysis Code (RMAC) and these were provided as inputs to the acoustic propagation code PSU-WOPWOP to evaluate the acoustic pressure time history at desired observer locations, considering thickness and loading noise sources from the various rotors. The acoustic pressure histories were in turn used to calculate overall sound pressure level (OASPL) and radiated acoustic power over an observer hemisphere. The simulation tools used in this study were validated against experimental and simulation results from NASA Langley Research Center and showed good agreement. From the simulations conducted in the present study the following key conclusions can be drawn:

1. For the quadcopter with orthogonal phasing, low noise regions are observed along the inter-boom bisectors, with reductions between 5-9 dB relative to the equivalent single rotor. No such directivity pattern was evident with tip-to-tip phasing. Differences between the noise lows along orthogonal inter-boom bisectors were explained on phasing between acoustic signals from different rotor pairs. Despite the noise directivity (or lack thereof), the total radiated acoustic power (PWL) over the observer hemisphere appeared to be comparable between the orthogonal and tip-to-tip phasing cases.
2. For the hexacopter with orthogonal phasing, noise reductions of up to 9.5 dB are observed along alternate inter-boom bisectors, relative to the equivalent single rotor. A strong directivity pattern was also observed with tip-to-tip phasing. For the octocopter with orthogonal phasing, 13-14 dB noise reductions are observed along inter-boom bisectors, but like the quadcopter directivity in propagated noise was absent for tip-to-tip phasing. For both the hexacopter and octocopter, orthogonal phasing shows a reduction total radiated acoustic power (PWL)

relative to the equivalent single rotor, while tip-to-tip phasing shows an increase.

3. As the number of rotors increases, the smaller, faster spinning rotors have more tonal peaks at progressively higher frequencies on overall sound pressure level frequency spectra. As a consequence, A-weighting significantly penalizes the smaller, faster-spinning rotors, regardless of orthogonal or tip-to-tip phasing.
4. The effect of change in disk loading on the radiated noise was examined for the quadcopter. When the tip Mach number was increased to achieve higher disk loadings of 9lbs/ft^2 and 12lbs/ft^2 (while holding the rotor root pitch) the overall noise levels increased significantly and the low-noise regions along the inter-boom bisectors with orthogonal phasing (previously seen at 6lbs/ft^2) were no longer evident. Conversely, when the tip Mach number was decreased to achieve a disk loading of 3lbs/ft^2 the overall noise levels decreased significantly and the low-noise regions along the inter-boom bisectors became even more pronounced (with 18-25 dB reductions over the equivalent single rotor). Holding the tip Mach number (at 0.6) and changing disk loading through variation in root pitch had a much smaller effect on radiated noise levels, and quiet regions along inter-boom bisectors with orthogonal phasing were not observed. Noise directionality with orthogonal phasing (low noise along inter-boom bisectors) appears strongest at low tip Mach numbers.

REFERENCES

1. Holden, J., and Goel, N., "Fast-Forwarding to a Future of On-Demand Urban Air Transportation." UBER Elevate Whitepaper, October 2016, available at: https://www.uber.com/elevate.pdf [Accessed 10 Oct. 2019].
2. NASA, "NASA's UAM Grand Challenge," Aug. 2019, Available at: https://www.nasa.gove/uamgc [Acessed 10 Oct. 2019].
3. Swartz, K., "NASA Embraces Urban Air Mobility," Vertiflite Magazine, Jan-Feb 2019.
4. Schmitz, F., "The Challenges and Possibilities of a Truly Quiet Helicopter: 29th Alexander A. Nikolsky Honorary Lecture," *Journal of American Helicopter Society*, Vol. 61, No.4, 2016, pp. 1-33.
5. Zawodny, N., Boyd, D. D., and Burley, C., "Acoustic Characterization and Prediction of Representative, Small-Scale Rotary-Wing Unmanned Aircraft System Components," *72nd Annual Forum of the American Helicopter Society,* West Palm Beach, FL, May 2016.
6. Zawodny, N., and Boyd, D. D., "Investigation of Rotor-Airframe Interaction Noise Associated with Small-Scale Rotary-Wing Unmanned Aircraft Systems," *73rd Annual Forum of the American Helicopter Society,* Fort Worth, TX, May 2017.
7. Pettingill, N. and Zawodny, N., "Identification and Prediction of Broadband Noise for a Small Quadcopter," *75th Annual Forum of the Vertical Flight Society,* Philadelphia, PA, May 2019.
8. Schiller, N., Pascioni, K., and Zawodny, N., "Tonal Noise Control using Rotor Phase Synchronization," *75th Annual Forum of the Vertical Flight Society,* Philadelphia, PA, May 2019.
9. Pascioni, K. A., Rizzi, S. A., and Schiller, N.H., "Noise reduction potential of phase control for distributed propulsion vehicles," Paper AIAA 2019-1069, AIAA SciTech Forum and Exposition Proceedings, San Diego, CA, January 2019.
10. Intaratep, N., Alexander, W., and Devenport, W., "Experimental Study of Quadcopter Acoustics and Performance at Static Thrust Conditions," *22nd AIAA/CEAS Aeroacoustics Conference*, Lyon, France, May 2016.
11. Tinney, C. and Sirohi, J., "Multirotor Drone Noise at Static Thrust," *AIAA Journal,* Vol. 56, No. 7, July 2018, pp. 2816-2826
12. Tinney, C. and Valdez, J., "Acoustic Scaling for Small Rotors in Hover," *75th Annual Forum of the Vertical Flight Society,* Philadelphia, PA, May 2019.
13. Passe, B. and Baeder, J., "Computational Aeroacoustics of Different Propeller Configurations for eVTOL Applications," *Vertical Flight Society's Autonomous VTOL Technical Meeting and Electric VTOL Symposium,* Mesa, Arizona, Jan. 2019.
14. Quackenbush, T., Wachspress, D., Moretti, L., Barwey, D., Lewis, R., and Brentner, K., "Aeroacoustic Modeling of an eVTOL Slowed Rotor Winged Compound Aircraft," *75th Annual Forum of the Vertical Flight Society,* Philadelphia, PA, May 2019.
15. Jia, Z., and Lee, S., "Acoustic Analysis of Urban Air Mobility Quadrotor Aircraft," *Vertical Flight Society's Transformative Vertical Flight Forum*, San Jose, CA, Jan 21-23, 2020
16. Wachspress, D., Yu, M., and Brentner, K., "Rotor/Airframe Aeroacoustic Prediction for eVTOL UAM Aircraft," *75th Annual Forum of the Vertical Flight Society,* Philadelphia, PA, May 2019
17. Zhang, J., Brentner, K., and Smith, E., "Prediction of the Aerodynamic and Acoustic Impact of Propeller-Wing Interference," *Vertical Flight Society's Transformative Vertical Flight Forum*, San Jose, CA, Jan 21-23, 2020.
18. Mukherjee, B., and Brentner, K., "Investigation of Propeller-Wing Interaction Noise and Potential Contribution to eVTOL Noise," *Vertical Flight Society's Transformative Vertical Flight Forum*, San Jose, CA, Jan 2020.
19. Li, S., and Lee, S., "UCD-QuietFly: A New Program to Predict Multi-Rotor eVTOL Broadband Noise" *Vertical Flight Society's Transformative Vertical Flight Forum*, San Jose, CA, Jan 21-23, 2020.
20. Mankbadi, R. R., Afari, S. O., and Golubev, V. V., "Simulations of Broadband Noise of a Small UAV Propeller," AIAA SciTech 2020 Forum, 6-10 January 2020, Orlando, FL, https://doi.org/10.2514/6.2020-1493.
21. Walter, A., McKay, M., Niemiec, R., Gandhi, F., and Ivler, C., "Handling Qualities Based Assessment of

Scalability for Variable-RPM Electric Multi-Rotor Aircraft," *75th Annual Forum of the Vertical Flight Society*, Philadelphia, PA, May 2019.
22. Bahr, M., McKay, M., Niemiec, R., and Gandhi, F., "Performance and Handling Qualities Assessment of Large Variable-RPM Multi-Rotor Aircraft for Urban Air Mobility," *76th Annual Forum of the Vertical Flight Society,* Montreal, Canada, May 2020.
23. Walter, A., McKay, M., Niemiec, R., Gandhi, F., Ivler, C., "Disturbance Rejection and Handling Qualities of Fixed-Pitch, Variable-RPM Quadcopters with Increasing Rotor Diameter," *76th Annual Forum of the Vertical Flight Society,* Montreal, Canada, May 2020.
24. Niemiec, R., Gandhi, F., Lopez, M., and Tischler, M., "System Identification and Handling Qualities Predictions of an eVTOL Urban Air Mobility Aircraft Using Modern Flight Control Methods," *76th Annual Forum of the Vertical Flight Society,* Montreal, Canada, May 2020.
25. https://evtol.news/2020/01/15/joby-aviation-unveils-s4/, accessed February 21, 2020.
26. Kopyt, N., Niemiec, R., and Gandhi, F., "Quadcopter Rotor Phasing for Minimization of Aircraft Vibratory Loads," *Vertical Flight Society's Transformative Vertical Flight Forum*, San Jose, CA, Jan 21-23, 2020.
27. Kopyt, N., Niemiec, R., and Gandhi, F., "Optimal Rotor Phasing for Multicopter Vibratory Load Minimization," *76th Annual Forum of the Vertical Flight Society,* Montreal, Canada, May 2020.
28. Niemiec, R. and Gandhi, F., "Development and Validation of the Rensslaer Multicopter Analysis Code (RMAC): A Physics-Based Comprehensive Modeling Tool," *75th Annual Forum of the Vertical Flight Society,* Philadelphia, PA, May 2019.
29. Brentner, K., Bres, G. A., and Perez, G., "Maneuvering Rotorcraft Noise Prediction: A New Code for a New Problem," *AHS Aerodynamics, Acoustics, and Test and Evaluation Technical Specialist Meeting,* San Fransisco, CA, Jan. 2002.

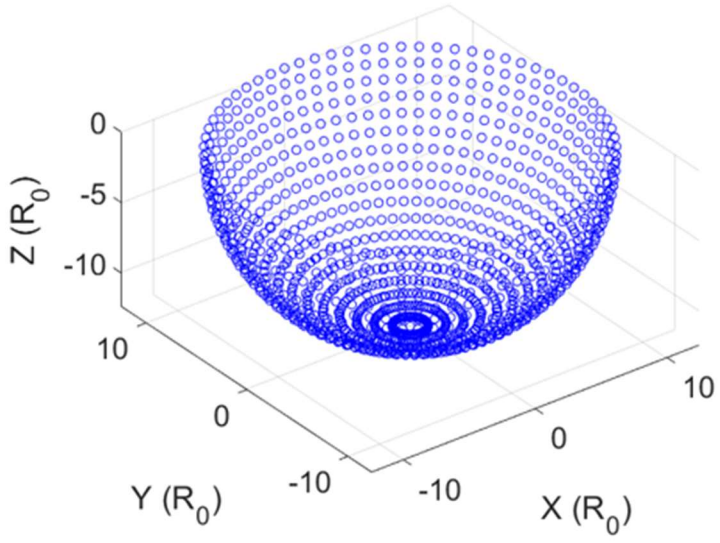

Figure 1: Hemisphere of radius $12.5R_0$, showing observer locations at 5 deg increments in azimuth and elevation angle

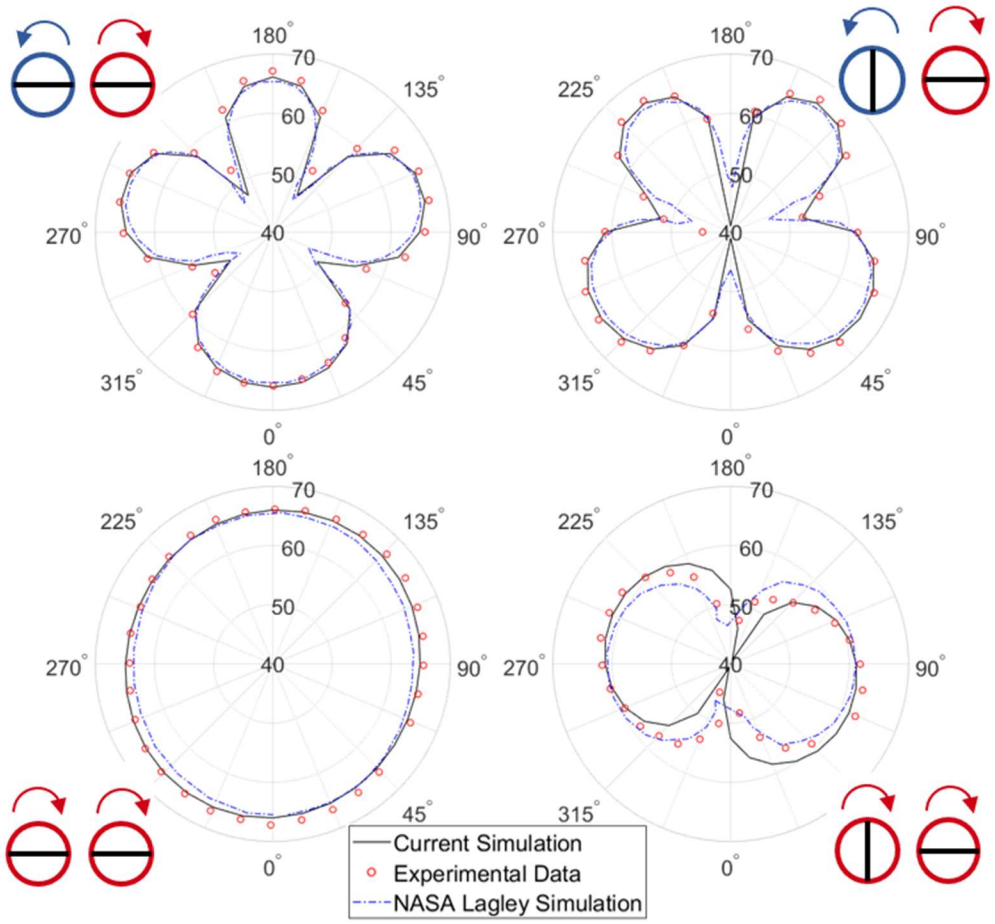

Figure 2: Validation of sound pressure level predictions at blade passage frequency in the plane of the rotors, versus NASA Langley experiment and simulation results

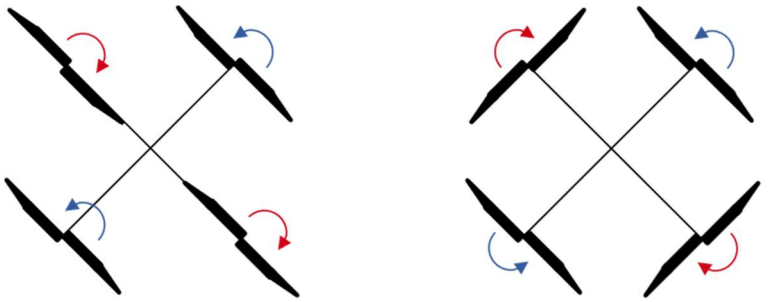

Figure 3: Quadcopter with orthogonal (left) and tip-to-tip (right) rotor phasing

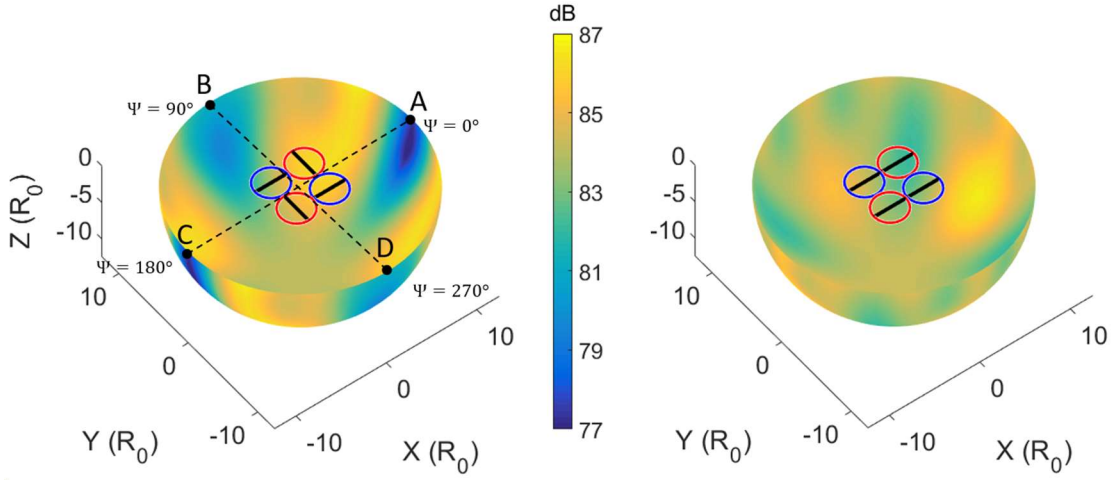

Figure 4: Overall Sound Pressure Level (OASPL) for quadcopter with orthogonal (left) and tip-to-tip (right) rotor phasing

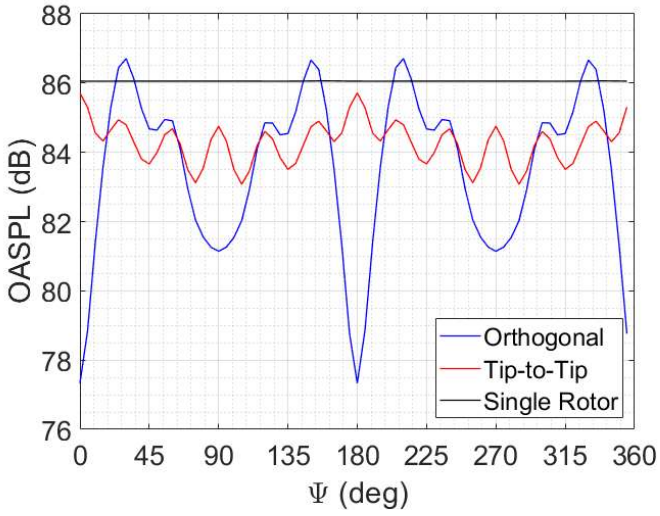

Figure 5: OASPL comparisons at 0 deg elevation for quadcopter with orthogonal and tip-to-tip rotor phasing

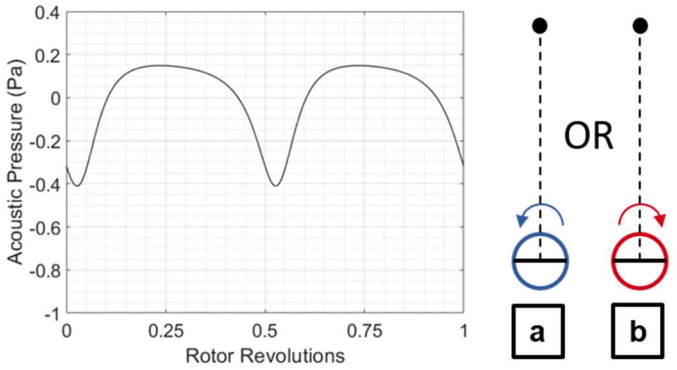

Figure 6: Acoustic pressure at in-plane observer on the hemisphere, from a single quadcopter at the origin

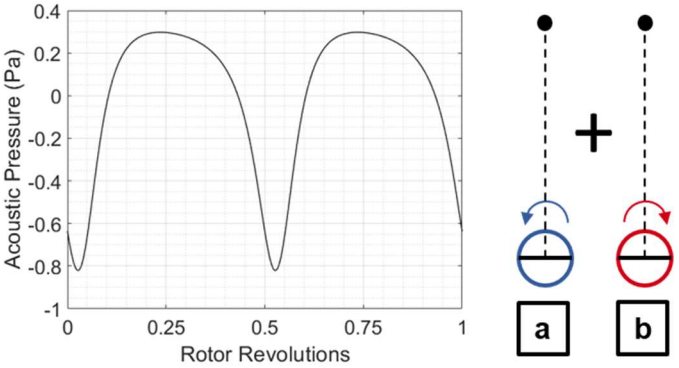

Figure 7: Acoustic pressure at in-plane observer on the hemisphere, from coincident CW and CCW quadcopter rotors at the origin with *tip-to-tip phasing*

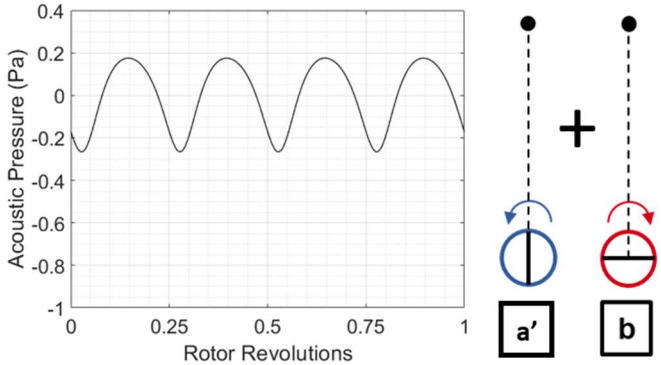

Figure 8: Acoustic pressure at in-plane observer on the hemisphere, from coincident CW and CCW quadcopter rotors at the origin with *orthogonal phasing*

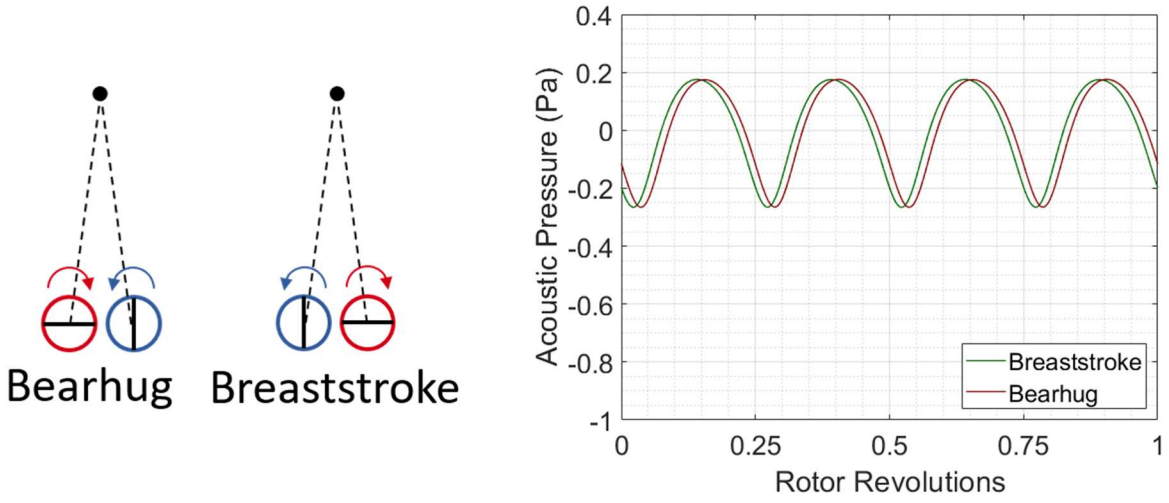

Figure 9: Two-rotor configurations: the *bearhug* and *breaststroke*

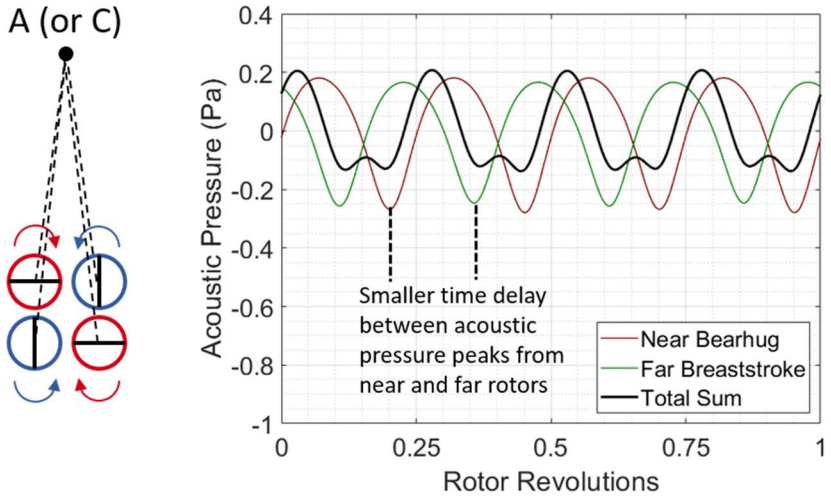

Figure 10: In-plane acoustic pressure at points A and C on hemisphere in Figure Q1 (near *bearhug* and far *breaststroke*)

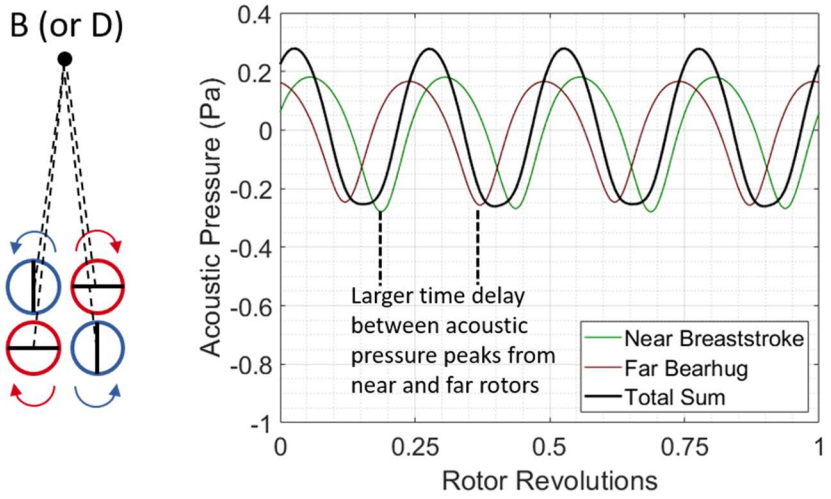

Figure 11: In-plane acoustic pressure at points B and D on hemisphere in Figure Q1 (near *breaststroke* and far *bearhug*)

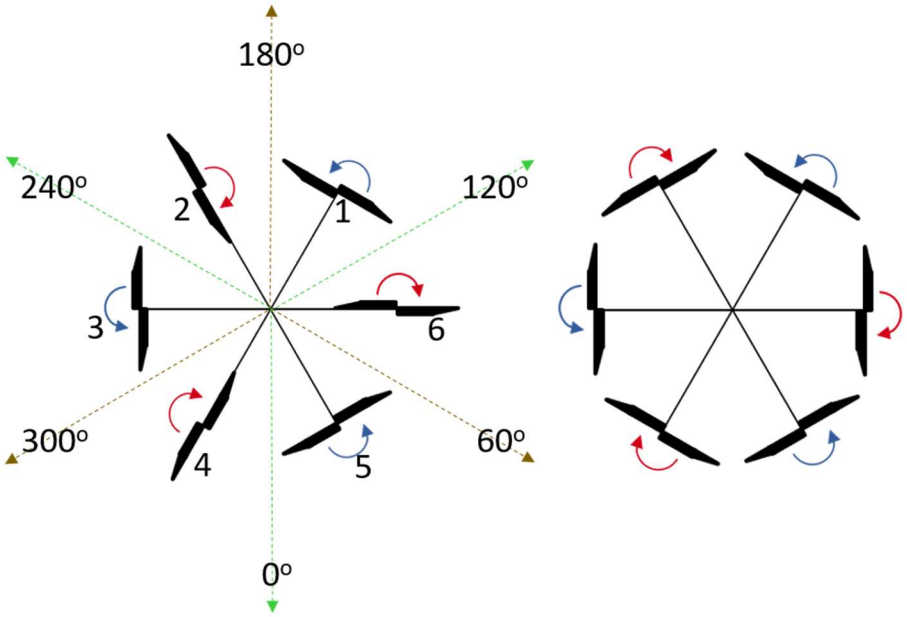

Figure 12: Hexacopter with orthogonal (left) and tip-to-tip (right) rotor phasing

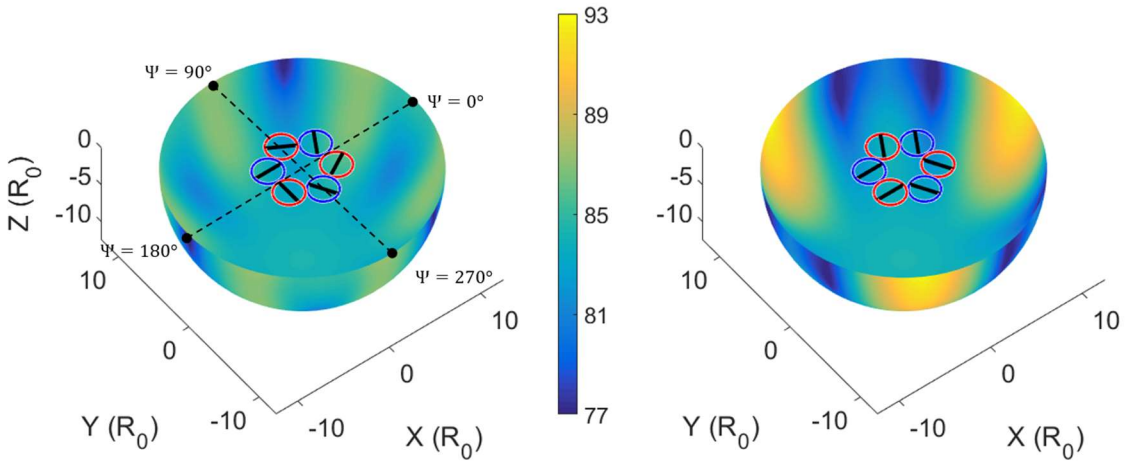

Figure 13: Overall Sound Pressure Level (OASPL) for hexacopter with orthogonal (left) and tip-to-tip (right) rotor phasing

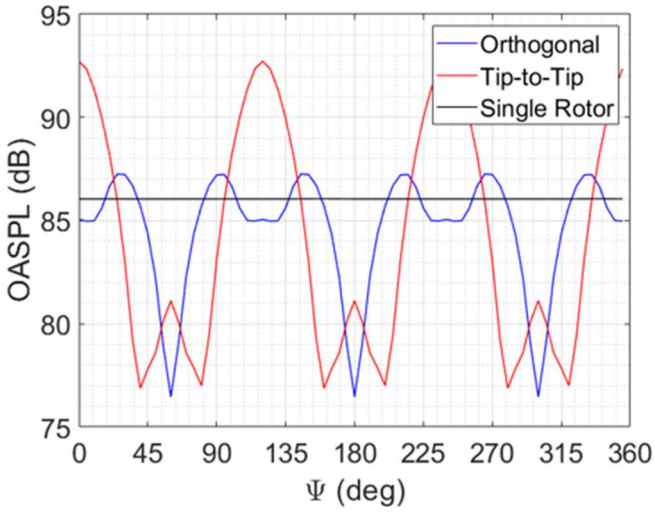

Figure 14: OASPL comparisons at 0 deg elevation for hexacopter with orthogonal and tip-to-tip phasing

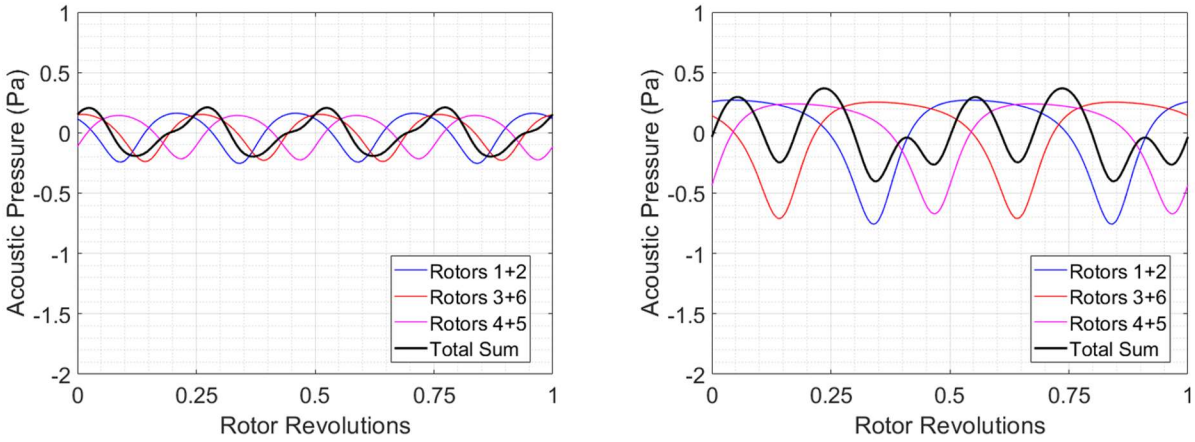

Figure 15: Acoustic pressure at in-plane observer along the 180° inter-boom bisector for a hexacopter with orthogonal (left) and tip-to-tip (right) rotor phasing

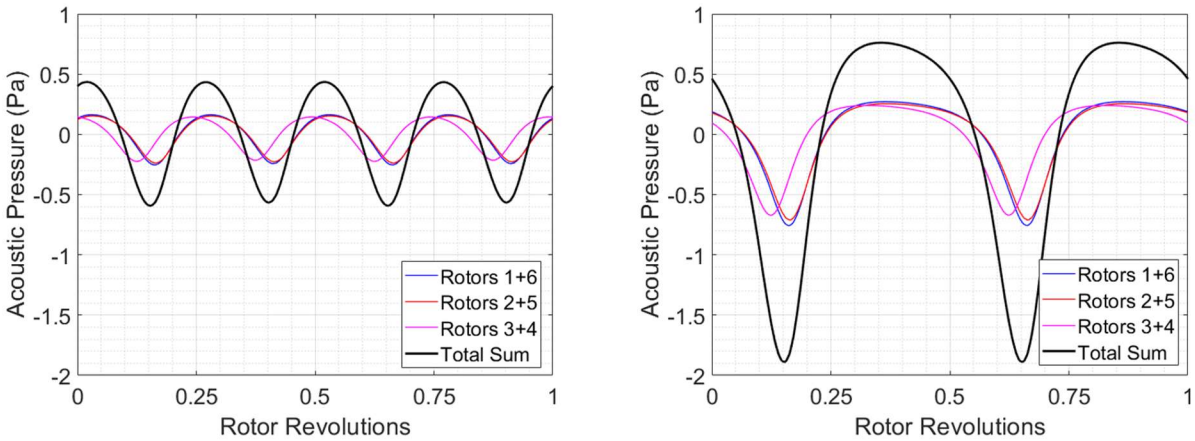

Figure 16: Acoustic pressure at in-plane observer along the 120° inter-boom bisector for a hexacopter with orthogonal (left) and tip-to-tip (right) rotor phasing

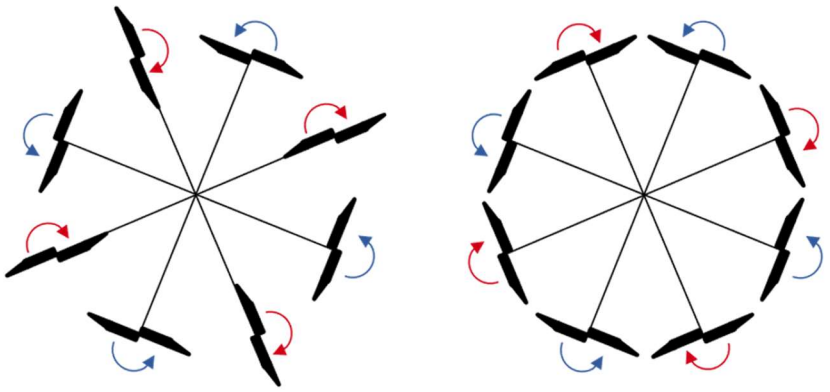

Figure 17: Octocopter with orthogonal (left) and tip-to-tip (right) rotor phasing

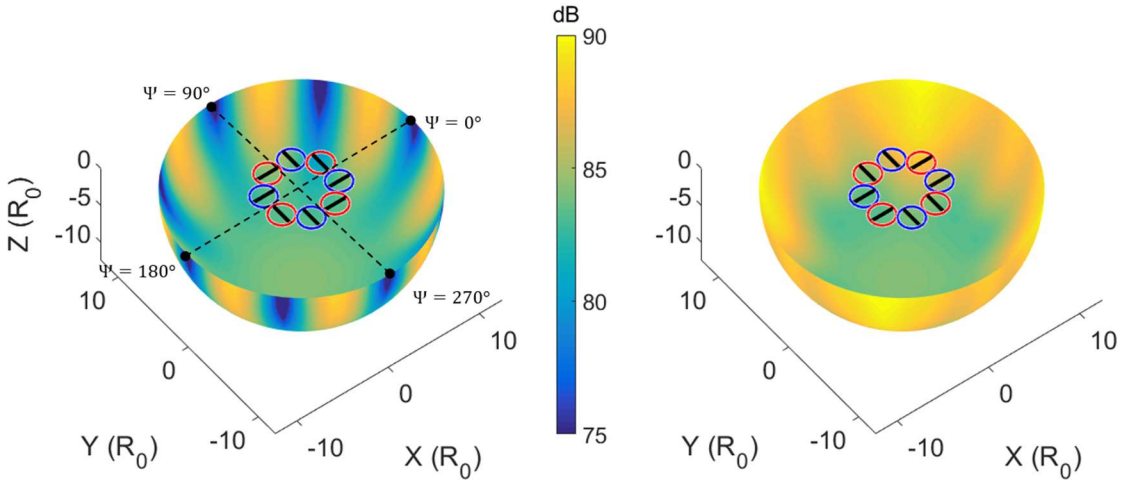

Figure 18: Overall Sound Pressure Level (OASPL) for octocopter with orthogonal (left) and tip-to-tip (right) rotor phasing

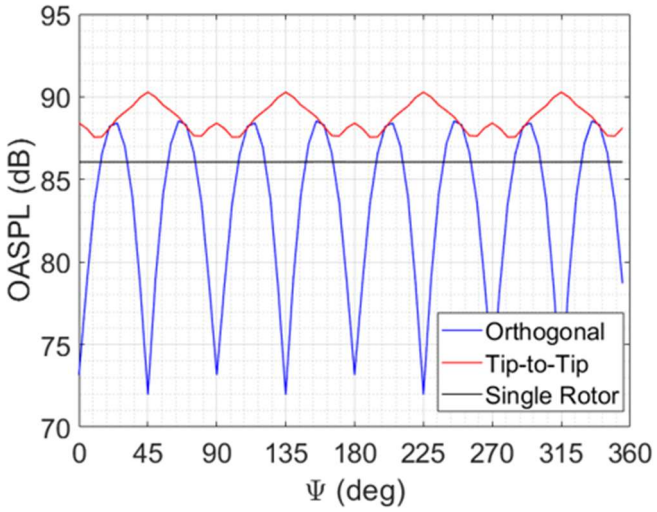

Figure 19: OASPL comparisons at 0 deg elevation for octocopter with orthogonal and tip-to-tip rotor phasing

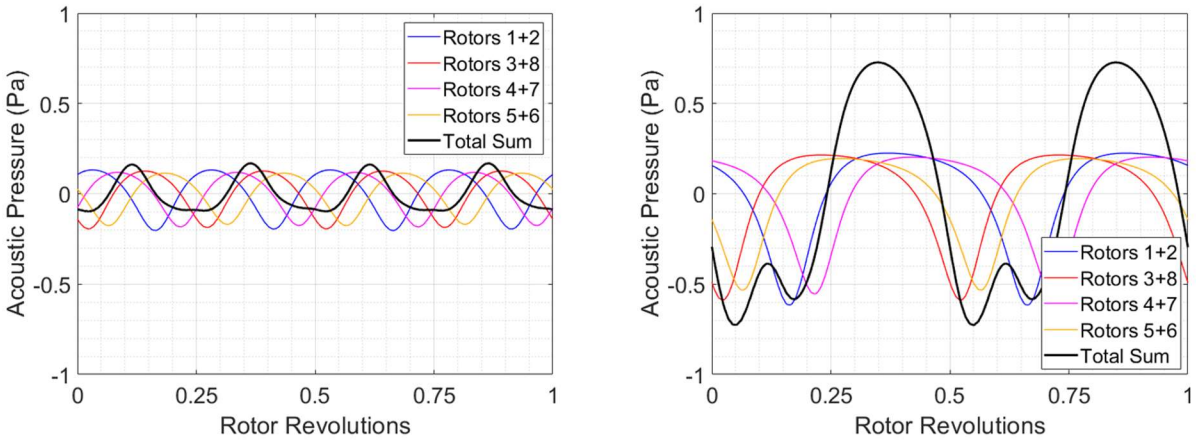

Figure 20: Acoustic pressure at in-plane observer along the 180° inter-boom bisector for an octocopter with orthogonal (left) and tip-to-tip (right) rotor phasing

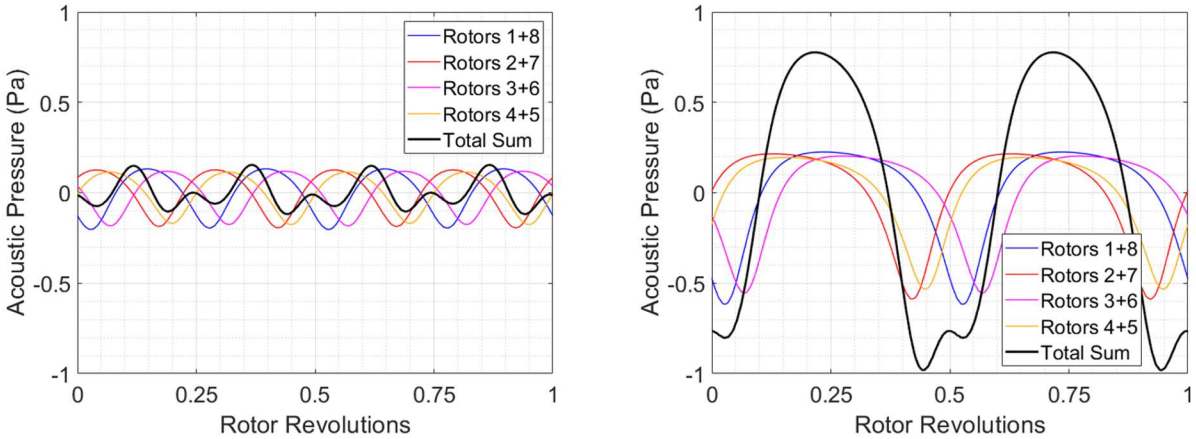

Figure 21: Acoustic pressure at in-plane observer along the 135° inter-boom bisector for an octocopter with orthogonal (left) and tip-to-tip (right) rotor phasing

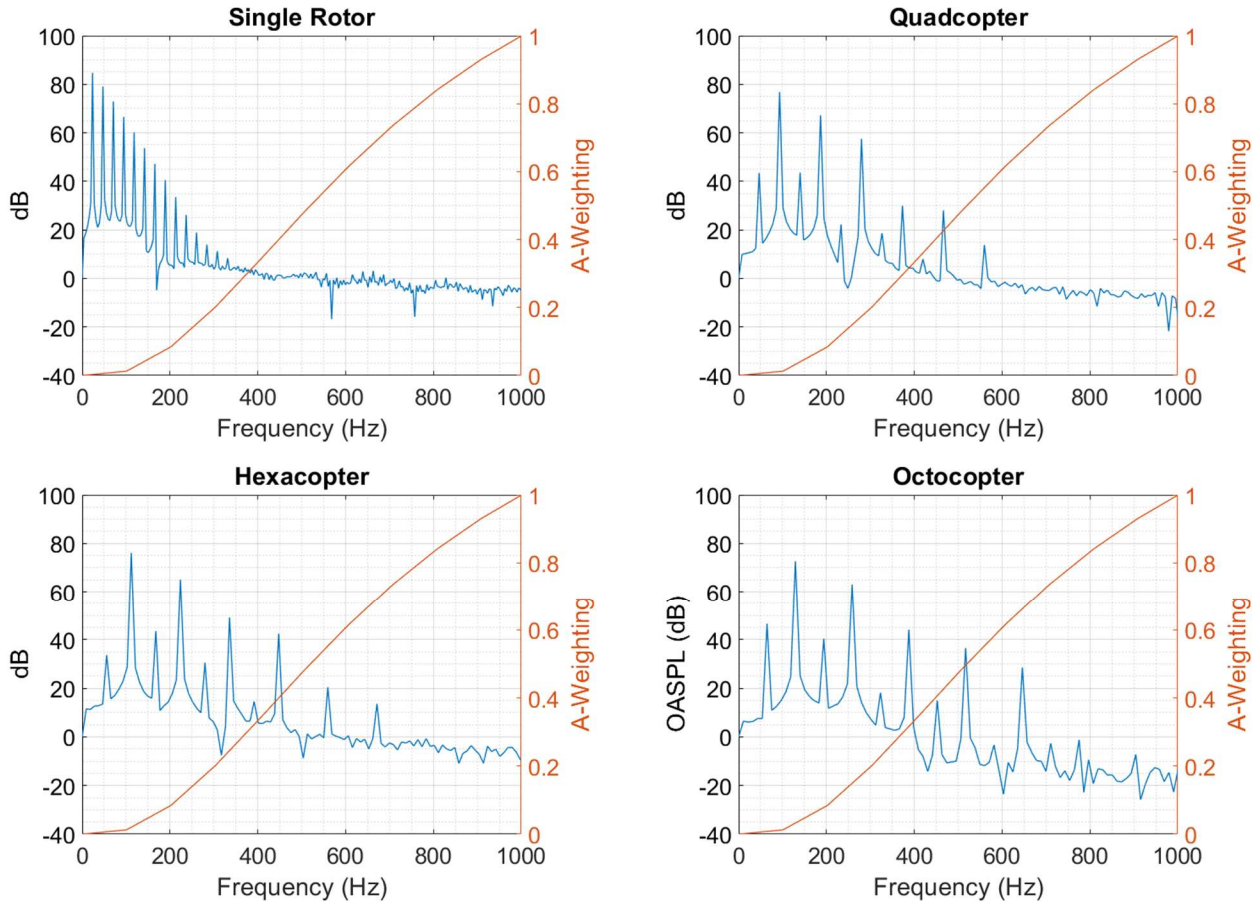

Figure 22: A comparison of frequency spectra of overall sound pressure levels for various multi-copter configurations

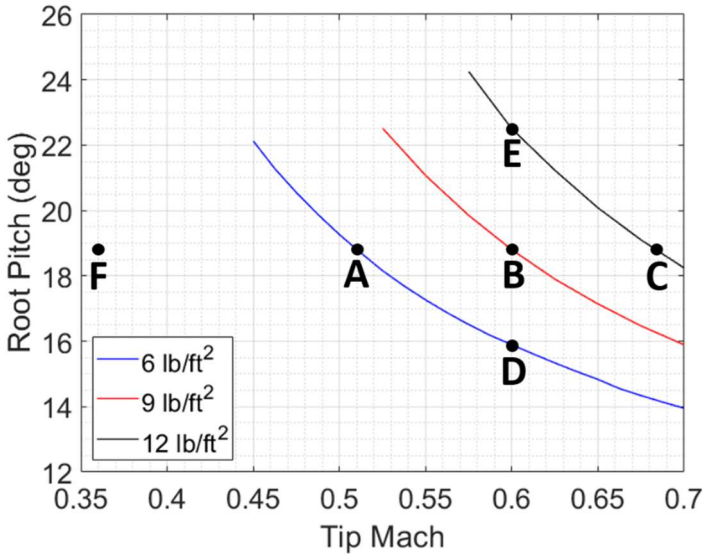

Figure 23: Variation of disk loading with tip Mach number and root pitch

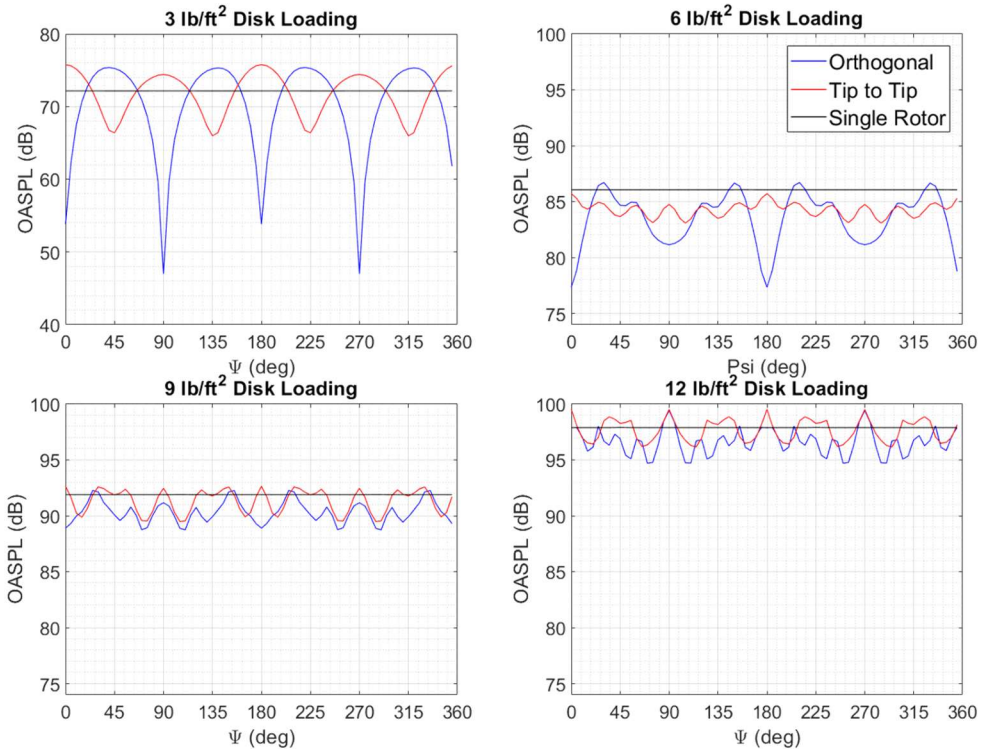

Figure 24: In-plane OASPL for increasing disk loading with increasing tip Mach number (constant root pitch of 18.8 deg)

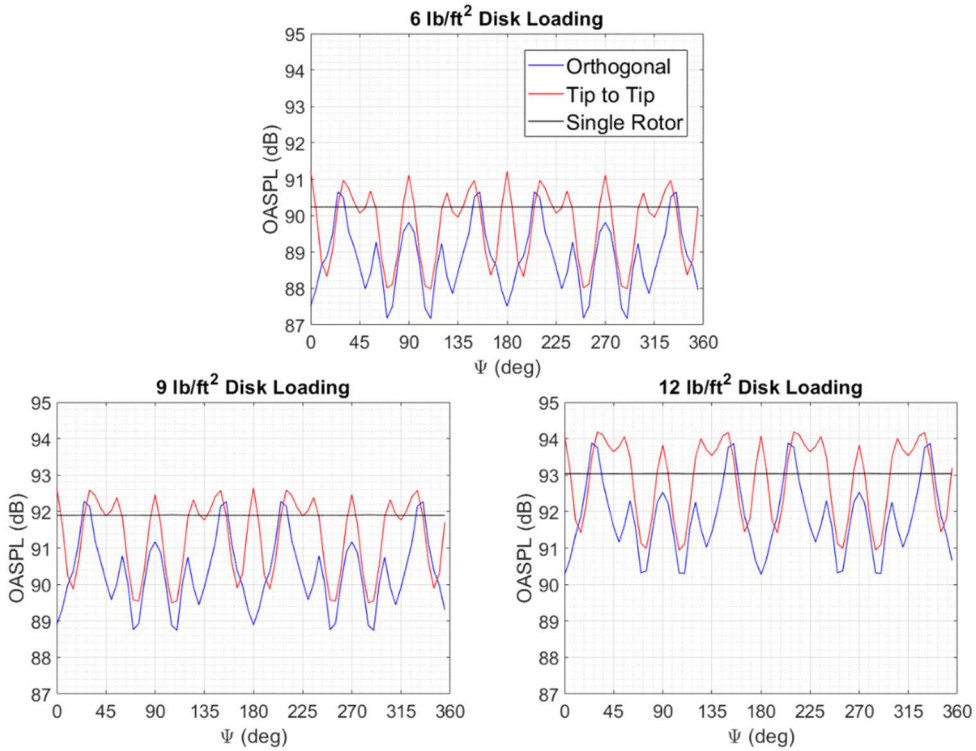

Figure 25: In-plane OASPL for increasing disk loading with increasing root pitch (constant tip Mach number of 0.6)

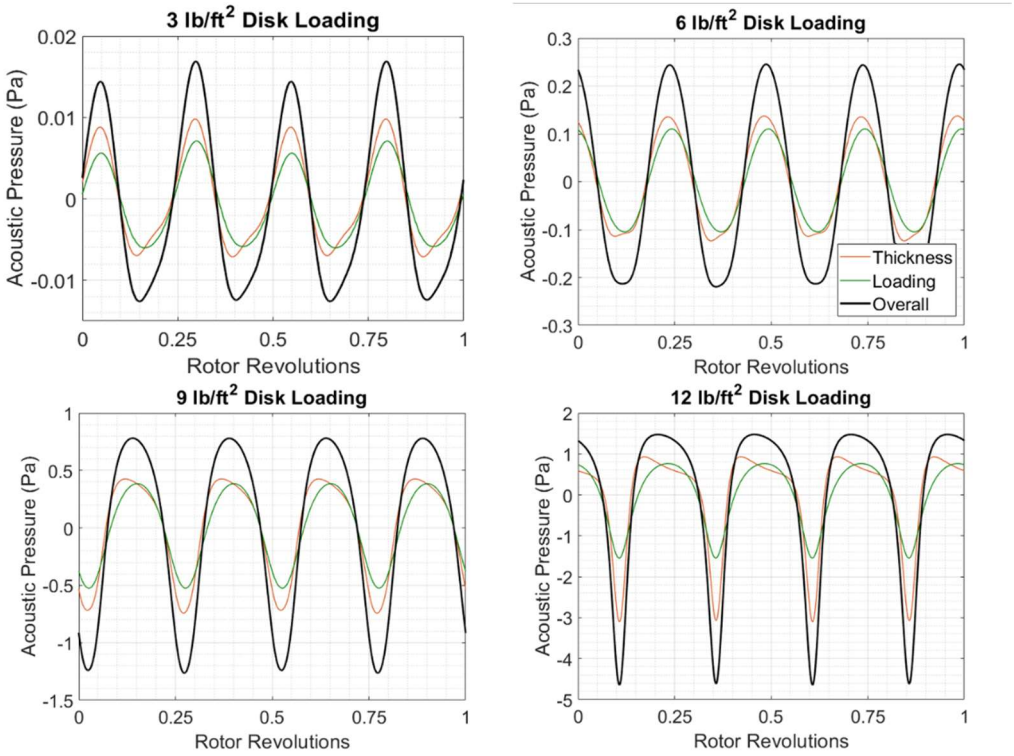

Figure 26: Acoustic pressure signals, and their decomposition at an in-plane observer along the 90 deg inter-boom bisector, for increasing disk loading with increasing tip Mach number (constant root pitch of 18.8 deg)

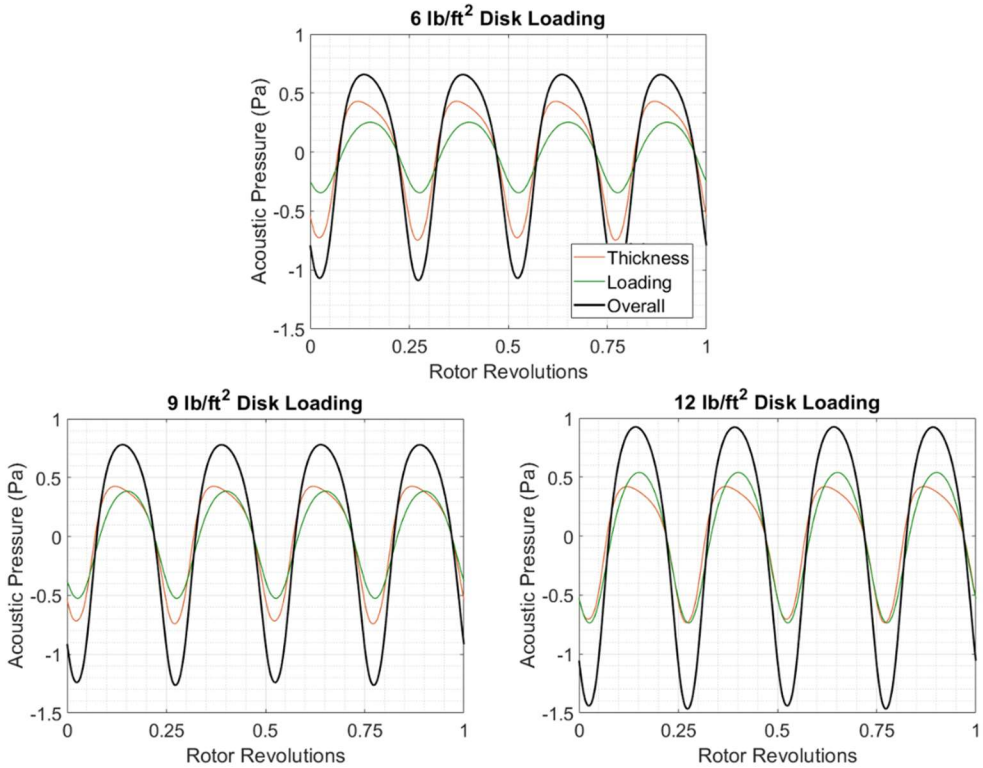

Figure 27: Acoustic pressure signals, and their decomposition at an in-plane observer along the 90 deg inter-boom bisector, for increasing disk loading with increasing root pitch (constant tip Mach number of 0.6)

Table 1: Rotor Radius and RPM for various multi-copter configurations

	Single Rotor	Quad	Hex	Oct
Radius	2.438 m [8 ft]	1.219 m [4 ft]	0.995 m [3.226 ft]	0.862 m [2.828 ft]
RPM	685.5	1371	1679	1939

Table 2: Radiated power over partial hemisphere for co-rotating and counter-rotating assemblies with 0 and 90 deg phasing

Configuration	ΔPWL from Present Simulations (dB)	ΔPWL from Ref. 8 Simulations (dB)	ΔPWL from Ref. 8 Experiment (dB)
Counter, $\psi_r = 0°$	-0.136	0.2	0.4
Counter, $\psi_r = 90°$	-0.0075	-0.1	-0.3
Co, $\psi_r = 0°$	2.312	2.3	2.5
Co, $\psi_r = 90°$	-5.211	-5.2	-5.8

Table 3: Acoustic power radiated over the observer hemisphere (PWL) for the various multi-copter configurations relative to the single rotor

	Orthogonal	Tip-to-Tip
Quadcopter	-0.74 dB	-0.64 dB
Hexacopter	-0.30 dB	1.04 dB
Octocopter	-0.70 dB	2.02 dB

Table 4: Acoustic power comparisons over the observer hemisphere with application of A-weighting relative to the single rotor

	Orthogonal	Tip-to-Tip
Quadcopter	8.16 dB	9.36 dB
Hexacopter	10.76 dB	11.72 dB
Octocopter	13.66 dB	15.07 dB